Molecular-dynamics studies of defect generation in epitaxial Mo/W superlattices

M. H. Carlberg, E. P. Münger, and V. Chirita
Department of Physics and Measurement Technology, Linköping Institute of Technology, S-58183 Linköping, Sweden
(Received 22 January 1996)

An investigation of defect generation at the interface during growth of epitaxial (100) oriented Mo/W superlattices by ion-assisted deposition has been carried out using molecular-dynamics simulations. The influence of the impact parameter within the irreducible bcc unit cell [001] surface and the incident ion energy on the energy accommodation, the dynamics of energy transfer, and energy dissipation are discussed. A detailed model of the generation of point defects is presented and the influence of materials upon the type and the number of defects as well as the energy accommodation of the superlattice is revealed. It is shown that the behavior of the superlattice as a whole is largely dominated by the material in the surface monolayer. [S0163-1829(96)03627-2]

I. INTRODUCTION

The synthesis of metallic superlattices (SL) with desired mechanical, optical, and electrical properties depends ultimately upon the profound understanding of the fundamental phenomena governing the growth of these structures. Interface roughness, interdiffusion, the generation of point defects and grain boundaries, stress levels, and relaxation are processes that will greatly affect the use of superlattices in applications such as magneto-optical media, magnetic recording heads, wear protective coatings, and electronic semiconductor devices. It is a well-known fact that today, due to technological requirements, most metallic superlattices are grown by dc magnetron sputtering,[1–5] a process that requires a sputtering gas, and as such, a process in which the bombardment with energetic particles plays an essential role during the growth process. During the deposition process, inevitably, gas atoms will be backscattered from the sputtering targets and will impinge on the growing surface, thus influencing various phenomena such as adatoms mobility, local temperature, generation of interfacial point defects, and many others.

The generation of interfacial point defects represents one of the critical phenomena occurring during the growth of metallic superlattices, as well as of ion-assisted thin films in general. The type and/or concentration of point defects will affect the physical properties of thin films, while at the interfaces in superlattices, the generation of point defects can result in interfacial mixing of the two atomic species, a process that ultimately leads to rough interfaces and/or irregularities in physical properties.[6–10] These effects have been studied extensively in Mo/V superlattices[11–13] grown by dual magnetron sputtering, and the results show that the interfacial defect generation processes are strongly connected to ion energy, dose and type, growth temperature, and material properties such as atomic mass, lattice, and/or elastic constants. The material properties are shown to be especially important in the sense that if the growing monolayers are formed by the heavier metal, they will exhibit a lower sputtering yield, as compared with its reported bulk values, whereas the situation is reversed when the lighter metal forms the growing monolayer. The explanation proposed by the authors was that the different mass ratios between the incoming ion and the two metallic species will affect the way in which energy is exchanged with the target surface.

In this paper we report a classical molecular-dynamics (MD) study of interfacial defect generation in Mo/W superlattices. In conjunction with experimental observations, computer simulations generally, and MD especially, give the opportunity to analyze the full dynamics of given phenomena and thus assist in formulating new theoretical models. The reason for choosing the Mo/W structure was that this is a good model system, as is characterized by a much better lattice match between the two atomic species, while the two mass ratios of interest, Ar/Mo and Mo/W, are almost equal. Also, in this structure, Mo is the lighter metal constituent; i.e., this system seemed well fit to probe the previously proposed model. For the same reasons, experimental work[14,15] has started on the same system, thus allowing for a direct comparison between MD and experimental results. We investigated the influence of incident energy, material properties, and impact parameters on the creation of residual point defects. The motivation behind our work was the need for a detailed, at the atomic level, description of the mechanisms responsible for these phenomena and their dependence on the above-mentioned parameters.

II. METHODOLOGY

The simulations of ion-induced effects during growth of metallic superlattices were carried out for two different configurations at 1000 K. The first configuration consisted of a bulk portion of one metallic species with a single monolayer of the alternate material placed on top. Typically, the first configuration contained 3024 atoms placed in 21 layers of 12×12 atoms each. In the second configuration the monolayer was shaved off, leaving 2880 atoms of the bulk material arranged in 20 layers. The materials in the structures will henceforth be referred to as X/Y where X is the atomic species in the top layer and Y is the bulk metal.

The free surfaces were simulated by holding the two bottom layers fixed. The two layers directly above were used as a heat bath in which the velocities of the atoms were scaled to the desired temperature of 1000 K in each time step. The

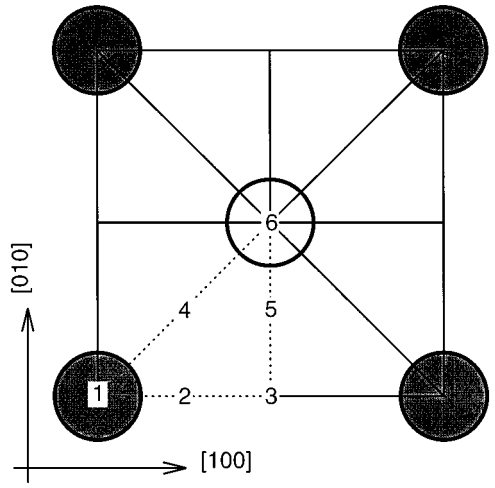

FIG. 1. Illustration of the bcc unit cell surface with the geometrically irreducible part marked by the dashed line. The six different impact points are marked by their numbers. ●, surface atom; ○, bulk atom.

atoms in the remaining layers were allowed to move freely according to the interaction potential. Initial oscillations were damped out and the box size was adjusted so as to get a zero mean pressure. Periodic boundary conditions were employed in the two directions parallel to the surface layer.

The simulation of atom bombardment was rendered by introducing single Ar atoms into the simulation box above the free surface, at a distance slightly larger than the cutoff distance of the gas-metal interaction potential used. The incoming atoms were normally incident on the six impact points chosen within the geometrically irreducible part of the [100] surface unit cell (Fig. 1). Kinetic energies of 50, 100, 150, and 200 eV where chosen for the incident Ar atom. A variable time step with the upper limit of 1 fs was used so that no atom in the simulation moved more than 0.01 Å /step, in order to achieve relatively short simulation times without affecting the energy conservation.

The metal-metal interactions were modeled using the embedded atom method[16] (EAM), which is based on density-functional theory. The total energy for the system is approximated by

$$E_{\mathrm{tot}}=\sum_i F_i(\rho_i)+\frac{1}{2}\sum_i \sum_{j\neq i} \phi_{ij}(r_{ij}). \tag{1}$$

Here $F(\rho_i)$ is the embedding function and ϕ_{ij} is the effective two-body interaction potential. The electron density ρ_i is approximated as a linear superposition of atomic electronic densities, computed from Hartree-Fock expansions[17] of the atomistic wave functions.

In this work two bcc metals, Mo and W, were studied using the special form of the EAM as developed by Johnson and Oh,[18] which has been shown to be equivalent to the original form proposed by Daw and Baskes.[16] The form of the embedding function is taken to be

$$F(\rho)=-(E_c-E_{1V}^{\mathrm{UF}})\left[1-\ln\left(\frac{\rho}{\rho_e}\right)^{1/8}\right]\left(\frac{\rho}{\rho_e}\right)^{1/8}, \tag{2}$$

TABLE I. Experimental constants used in fitting of the analytical forms of the interaction potentials for the two metals. E_c is the cohesive energy, a the lattice parameter, Ω the atomic volume, B the bulk modulus, G the Voight average shear modulus, A the anisotropy ratio, and E_{1V}^{UF} is the unrelaxed vacancy formation energy.

	Mo	W
E_c (eV) (Ref. 31)	6.810	8.66
a (Å) (Ref. 30)	3.150	3.16475
ΩB (eV) (Ref. 32)	25.68	30.65
ΩG (eV) (Ref. 32)	12.28	15.84
A (Ref. 32)	0.78	1.01
E_{1V}^{UF} (eV) (Refs. 33–35)	3.1	3.95

where E_c is the cohesive energy and E_{1V}^{UF} is the unrelaxed vacancy formation energy. Note that the pair potentials ϕ_{ij} are the effective pair potentials since the slope of the embedding function is zero, $F'(\rho_e)=0$, at the equilibrium electron density, ρ_e. The pair potential was taken as a cubic polynomial with an interaction range extending over nearest and next-nearest neighbors. For distances less than the nearest-neighbor equilibrium distance, r_{1e}, the pair potential was stiffened using[19]

$$\phi_a(r)=\phi(r)+k_a[\phi(r)-\phi(r_{1e})]\left(\frac{r}{r_{1e}}-1\right)^2, \tag{3}$$

$$k_a=4.5\left(1+\frac{4}{A-0.1}\right), \tag{4}$$

where A is the anisotropy ratio. The parameters in the analytical forms of the potentials are obtained by fitting the experimental data given in Table I.[18]

The interaction between different metallic atomic species was modeled using the weighted arithmetic mean of single species potentials:[19]

$$\phi_{X-Y}=\frac{f_Y(r)}{f_X(r)}\phi_{X-X}+\frac{f_X(r)}{f_Y(r)}\phi_{Y-Y}, \tag{5}$$

where $f_{X,Y}(r)$ is the electronic density at a distance r from atom X and ϕ_{X-X}, ϕ_{Y-Y} are the pair potentials for two atoms of type X and type Y, respectively. For computing efficiency the electronic density function f and the effective pair potentials were tabulated in the code and actual values computed as needed using cubic splines.

Interactions between the noble gas atoms and metallic atoms were described using a Lennard-Jones–type potential. Parameters were obtained from data for the pure materials using the Lorentz-Berthelot rules:[20]

$$\sigma_{XY}=\tfrac{1}{2}(\sigma_X+\sigma_Y), \tag{6a}$$

$$\epsilon_{XY}=\sqrt{\epsilon_X\epsilon_Y}. \tag{6b}$$

The computed values as such are listed in Table II.

To avoid a discontinuity at the cutoff of the interaction, a cubic spline was used between $r_c=r_{2e}+0.9(r_{3e}-r_{2e})$ and $r_s=r_{2e}+0.5(r_{3e}-r_{2e})$ for ρ and ϕ, where r_{2e} and r_{3e} are the equilibrium distances to the second and third neighbors.

TABLE II. Lennard-Jones interaction parameters computed from the cohesive energy, E_c (Ref. 18), and the lattice parameter, a_0 (Ref. 18), considering nearest and next nearest neighbors only.

Interaction	σ (Å)	ϵ (eV)
Ar-Ar	3.37	0.019
Mo-Mo	2.49	1.11
W-W	2.50	1.42
Ar-W	2.94	0.130
Ar-Mo	2.93	0.115

The simulation code was written in standard FORTRAN-77 and the simulations were carried out on a CRAY Y/MP-EL. One time step typically used 1–2 CPU seconds to complete. Dynamics of the simulation were visualized using an interactive graphic tool package developed by one of the authors.[22]

To study the effect of the simulation cell size, the number of atoms in each layer was increased from 12×12 to 36×36 for a total of 27 216 atoms. This simulation was carried out for Mo/W and incident atom energy of 200 eV. We found that, for the chosen configuration, qualitatively there were no differences in the results as obtained for the corresponding smaller system. As a further check of the quality of the simulation, the mean square displacements were monitored for each material simulated. From these, bulk and surface Debye temperatures were calculated. The values obtained are in good agreement with experimental data (Table III).

III. RESULTS

Typical defect generation events in the Mo/W structure due to bombardment with 200-eV Ar atoms are shown in Figs. 2 and 3. Each sequence of snapshots depicts the atoms participating in the process within a single layer cross section of the simulation cell. Figure 2 reproduces the effect of an impact between two atoms of the monolayer and between two atoms of the first bulk layer, i.e., impact point No. 3. The initial impact [Fig. 2(a)] has the effect of pushing the two atoms from the monolayer slightly downwards, towards the bulk layers, but mostly laterally, beneath their nearest neighbors in the monolayer [Fig. 2(b)]. At this time, the forward (downward) momentum of the initially affected monolayer atoms is reversed, and this results in sputtering one of their nearest neighbors in the monolayer. This is followed after $\sim$0.19 ps by the sputtering of the other nearest neighbor in the monolayer and one of the initially affected monolayer atoms [Fig. 2(c)], resulting in a final structure with three atoms missing [Fig. 2(d)]. The total time for this sequence of events to occur is approximately 0.4 ps. Figure 3 illustrates the effect of an impact between two atoms from the monolayer but straight on one of the atoms in the first bulk layer

TABLE III. Debye temperatures.

Material	Bulk (K)[a]	Surface (K)[b]	Experimental bulk values (K) (Ref. 21)
Mo	400	332	380
W	330	270	310

[a]Computed in this work.

[b]Computed in this work. Figure is an average over three top layers.

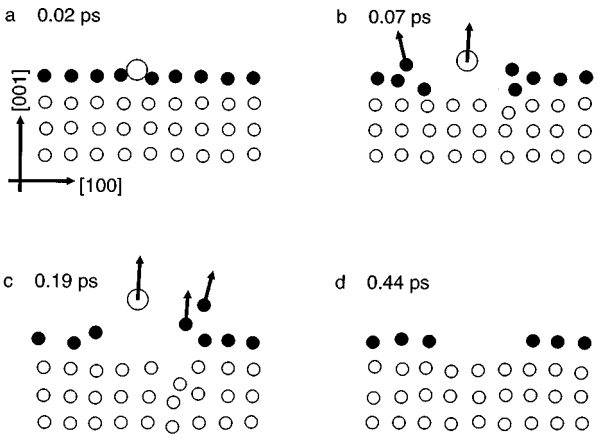

FIG. 2. The dynamics of surface roughening due to impact at point No. 3 by a 200-eV Ar atom on a Mo/W structure. A thin slab has been cut out of the three-dimensional simulation box and a time sequence of snapshots is shown. Note that three of the surface atoms from the top monolayer are sputtered. The arrows show the direction some atoms move, but are not scaled to the velocity. ●, Mo atom; ○, W atom; ○, Ar atom.

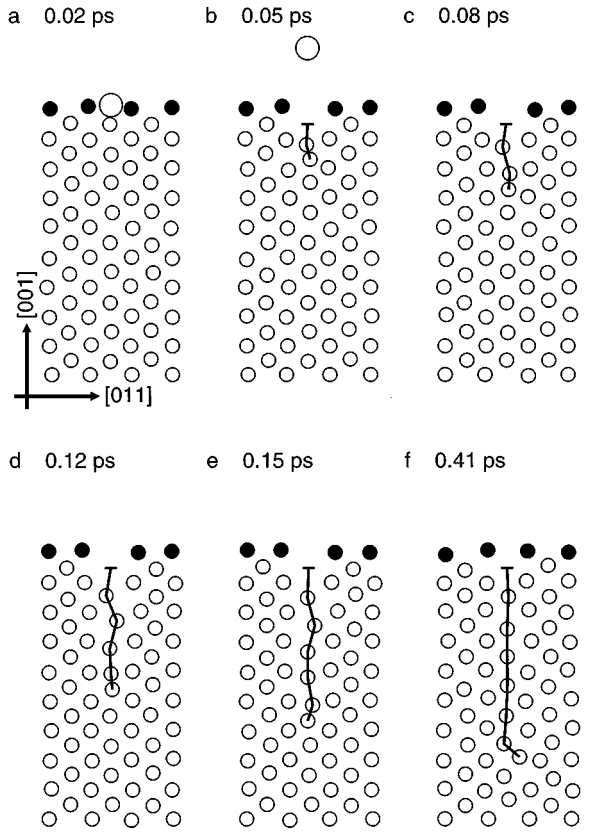

FIG. 3. Generation of an intrinsic residual defect (a Frenkel pair) during the simulation for impact point No. 6 on the Mo/W structure and for the Ar atom having the kinetic energy of 200 eV. The line drawn through some atoms marks the atoms involved in the process. ●, Mo atom; ○, W atom; ○, Ar atom.

(direct hit), i.e., impact point No. 6. In this case, the initial impact [Fig. 3(a)] has the effect of pushing the atom from the first bulk layer straight downwards, almost without affecting any of the atoms in the monolayer [Fig. 3(b)]. The downward momentum transferred to the atom in the first bulk layer following the initial impact is transmitted in turn to atoms lying directly underneath in a billiard-ball-like sequence [Figs. 3(c), 3(d), and 3(e)]. The final result of the impact is an interstitial, in the 14th bulk layer, i.e., at a distance of about 20 Å (7 unit cells) from the initial impact point [Fig. 3(f)]. The total time elapsed during this sequence of events is roughly the same as for the impact at point No. 3, i.e., approximately 0.4 ps.

In order to analyze the contrasting behavior of the impact points, we have examined the dynamics of the kinetic energy transfer to the individual layers of the superlattice. Figures 4 and 5 present energy dissipation as a function of time and depth in the superlattice for impact points 3 and 6, respectively. By examining Figs. 4(a) and 5(a) it can be seen that the superlattice absorbs the impact energy in the same time, approximately 0.20 ps. However, the mechanism of dissipation is totally different for the impact points. Following the impact at point 3, the energy is diffused mainly within the first four layers whereas for the other impact point a rapid energy transfer from the monolayer to the deeper layers of the superlattice is observed. This is due to the fact that at impact point 3, most of the energy is transmitted via the parallel component (144 eV) and very little (44 eV) via the normal component as shown in Figs. 4(b) and 4(c). The situation is exactly the opposite at impact point 6 [Figs. 5(b) and 5(c)], 9 and 94 eV for the parallel and normal component, respectively. The mechanism of energy dissipation described above confirms the importance that the impact parameter has in the growth process. At impact point 3 the Ar atom strikes between two nearest-neighbor surface atoms thereby pushing them apart, giving the parallel energy transfer. On the contrary, at impact point 6, the Ar atom strikes between two next nearest neighbors in the surface and directly on an atom in the first bulk layer, which has the effect of mostly normal energy transfer. Our results show that impact point 1 behaves as point 6, while 2, 4, and 5 exhibit intermediate behavior between the two extremes of impact points 3 and 6. Based on the energy transfer mechanism observed in our simulations, we conclude that, during growth, direct hits will most likely produce deep lying residual defects while in-between hits will most likely create residual defects in the growth surface.

A summary of the different types of defects obtained from our simulations, of Mo/W and W/Mo with Ar energies between 50 and 200 eV, indexed as intrinsic and extrinsic point defects, is presented in Fig. 6. The classification of intrinsic and/or extrinsic defects refers to defects involving atoms combined with interstitials and/or vacancies of the same material, while the latter involves atoms of two different atomic species,[23] Mo and W in this case. For the pure materials, the distinction between extrinsic and intrinsic defects is possible in MD by labeling the atoms of the surface layer. Only defects residing in the surface monolayer and the two layers immediately below the surface are considered, as this is generally viewed as the interface region in a growing superlattice. The results point to the fact that both intrinsic and extrinsic residual defects are generated either as single or as a

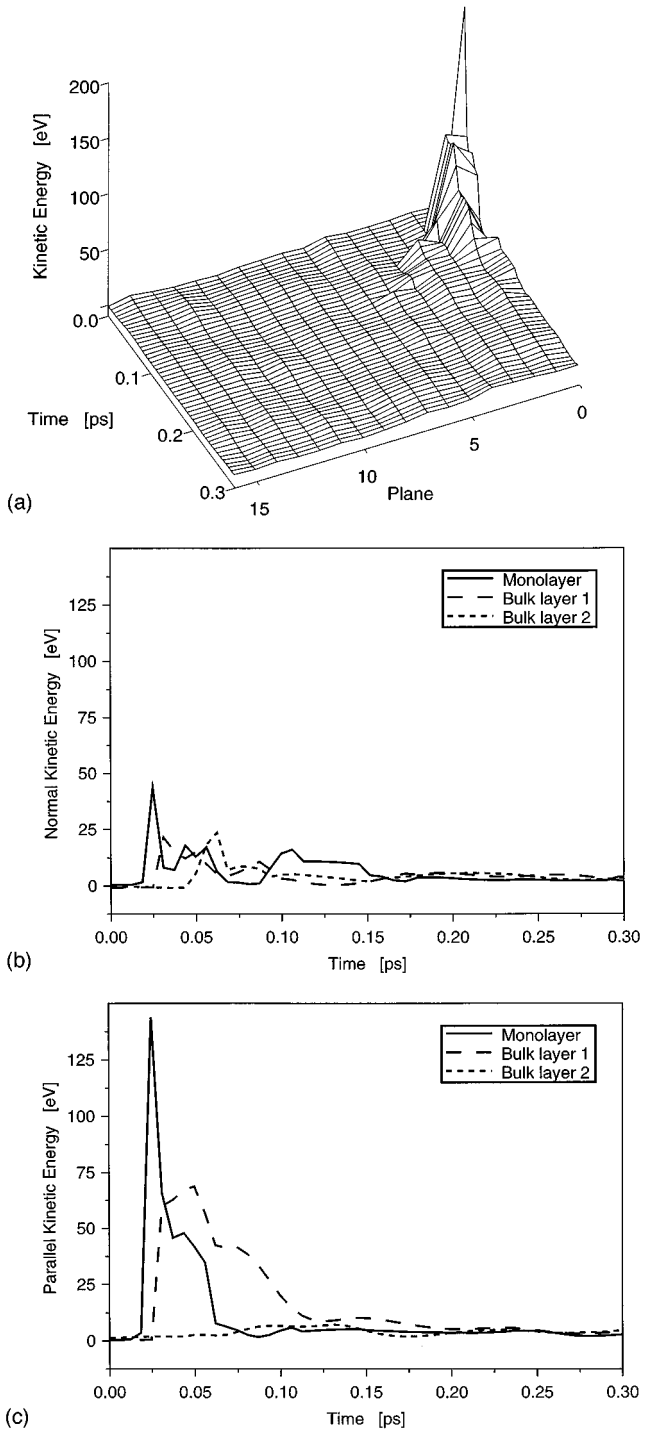

FIG. 4. (a) Time evolution and depth profile of the total kinetic energy transferred to the superlattice struck by 200-eV Ar atoms at impact point No. 3. Layer 0 is the monolayer. (b) Normal component of kinetic energy transferred to the superlattice due to impact at point No. 3. (c) Parallel component of kinetic energy transferred to the superlattice due to impact at point No. 3.

combination of point defects. Thus, at lower incident energies (less than 150 eV), only single point defects are generated, namely, intrinsic-Schottky-like [Fig. 6(a)], extrinsic substitutional [Fig. 6(b)], and intrinsic [sputtering from the monolayer, Fig. 6(c)]. As the incident energy increases above 150 eV, combinations of point defects occur as shown

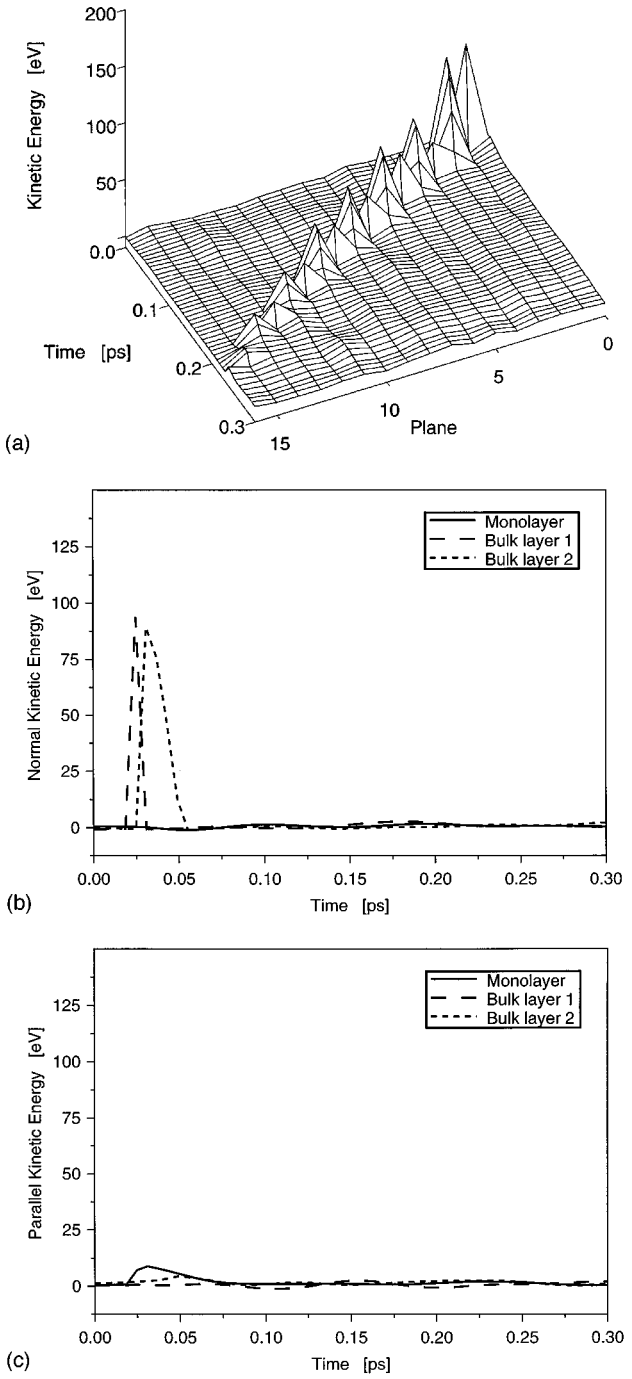

FIG. 5. (a) Time evolution and depth profile of the total kinetic energy transfered to the superlattice struck by 200-eV Ar atoms at impact point No. 6. (b) Normal component of kinetic energy transferred to the superlattice due to impact at point No. 6. (c) Parallel component of kinetic energy transferred to the superlattice due to impact at point No. 6.

in Figs. 6(d), 6(e), and 6(f). It should also be noted here that several different types of residual defects can occur in the same simulation, for example, the types shown in Figs. 6(c), 6(d), and 6(e). Analyzing the curves of the total number of defects, Fig. 7, one can observe that for both Mo/W and W/Mo there is generally an increase in the number of defects as the incident energy increases from 50 to 200 eV. However, this trend is more evident for the Mo/W structure as compared to the opposite one, and even more apparent when

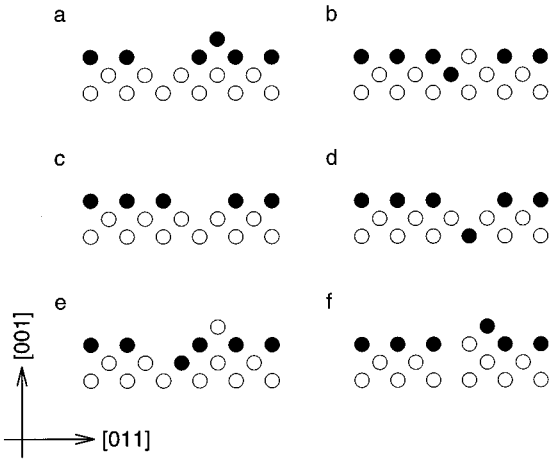

FIG. 6. Different types of residual defects as obtained from our simulations. (a) Intrinsic, Schottky-like. (b) Extrinsic, substitional. (c) Intrinsic, sputtering. (d) Extrinsic, substitutional, and Schottky-like. (e) Extrinsic, 2 substitutional, and Schottky-like. (f) Extrinsic, substitutional, and Schottky-like. For the pure materials, the distinction between extrinsic and intrinsic defects is possible in MD by labeling the atoms in the surface monolayer.

examining extrinsic defects only (Fig. 8).

In order to explain the different trends exhibited by the two structures, we have examined the transfer of energy from the incoming atom to the superlattice. A useful quantity in measuring the transfer of energy in gas-surface interactions is the energy accommodation coefficient (EAC) as defined by[24]

$$\alpha_e = \frac{\overline{E_{\mathrm{tot},f}} - \overline{E_{\mathrm{tot},i}}}{\overline{E_{\mathrm{tot},s}} - \overline{E_{\mathrm{tot},i}}}. \tag{7}$$

where $\overline{E_{\mathrm{tot},f}}$ is the total energy for the atoms and/or molecules scattered from the surface, $\overline{E_{\mathrm{tot},i}}$ is the total energy for the incoming particles, while $\overline{E_{\mathrm{tot},s}}$ is the energy per atom of the surface. In this work EAC was calculated for single incoming Ar atoms using only Eq. (7), and $\overline{E_{\mathrm{tot},s}}$ was considered negligible as compared to $\overline{E_{\mathrm{tot},i}}$. This is consistent with

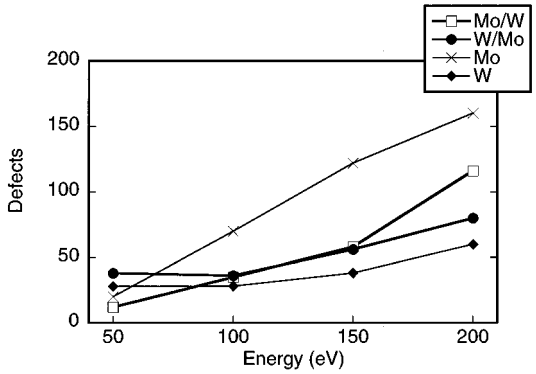

FIG. 7. Total number of intrinsic and extrinsic residual point defects, summed over the full bcc unit cell surface for the different material combinations used in this study.

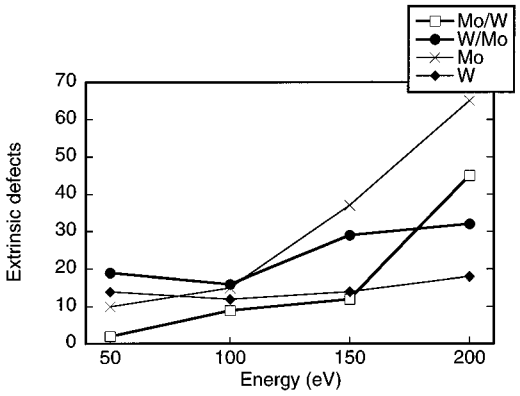

FIG. 8. Total number of extrinsic residual point defects only, summed over the full bcc unit cell surface for the different material combinations used in this study. For the pure materials, the distinction between extrinsic and intrinsic defects is possible in MD by labeling the atoms in the surface monolayer.

the simplified lattice model[25] for EAC in the limit of large kinetic energies of the incoming particles.

The dependence of the EAC's for the different material combinations, as a function of incident energy and impact point, can be seen in Figs. 9 and 10. From these figures it is evident that the transfer of energy is much more sensitive to the impact parameter in the case of the Mo/W structure, as compared with the W/Mo case. As there is basically no difference between the atomic radii of Mo and W and their elastic properties exhibit relatively small differences, this effect must be attributed to the different mass ratios of the atomic species, namely, 0.42 for Ar/Mo as compared with 0.22 for Ar/W. This effect is emphasized in Fig. 11, where the EAC's, averaged over all impact points, are plotted and compared with the EAC average values obtained for the single metal cases. The results are consistent with predictions of the hard-spheres model,[26–29] which gives the EAC as a function of only the mass ratio μ and the angle of incidence θ_i:

$$\alpha_e \approx 3.5\mu \cos\theta_i/(1+\mu)^2. \tag{8}$$

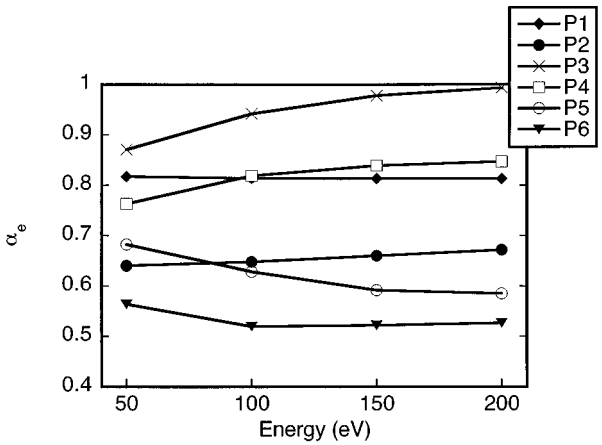

FIG. 9. EAC values for the different impact parameters and energies for the Mo/W structure.

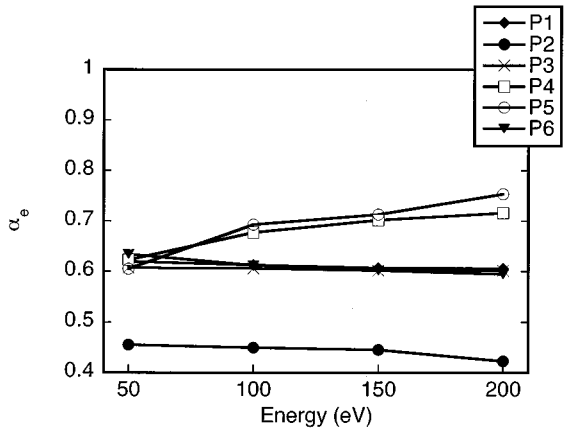

FIG. 10. EAC values for the different impact parameters and energies for the W/Mo structure.

The predicted values of the energy accommodation using Eq. (8) are 0.73 for Ar/Mo and 0.51 for Ar/W, whereas our simulations give 0.74 and 0.61. The higher value of EAC for Mo as compared to W translates into more energy transferred to the lattice. This means that more defects are expected to be created in Mo, which is indeed consistent with our results (see Figs. 7 and 8).

It is interesting to note that for both the Mo/W and W/Mo structures, the values of the EAC are drastically changed by the addition of the alternate material monolayer. This has the effect that the value of the EAC for the respective structure gets shifted towards the value of the same material as the monolayer when freely exposed to bombardment. In other words, in terms of EAC, the elastic and mass properties of the surface monolayer are largely determining the behavior of the whole structure.

However, in contrast to the single metal cases, the behavior of the values of the EAC does not translate directly into the number of defects generated for energies below 150 eV (Fig. 7). This effect is even more pronounced when examining the extrinsic defects only (Fig. 8). The W/Mo structure consistently exhibits more extrinsic defects, pointing to the fact that the generation of this type of defect is not affected in the same manner by the atomic mass ratio. Another dif-

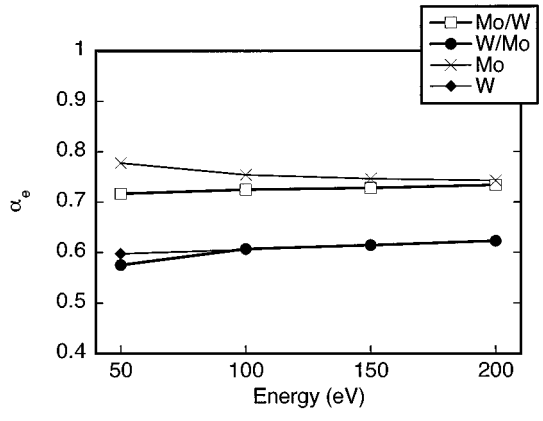

FIG. 11. EAC values for the different material combinations averaged over the full bcc unit cell surface.

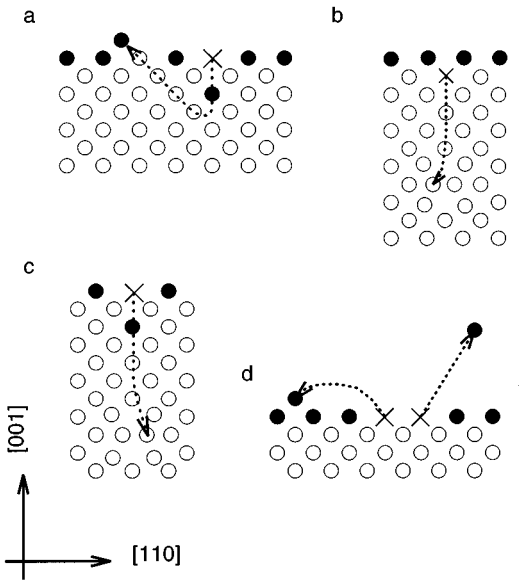

FIG. 12. Proposed models of residual point defect generation.

ference is that the Mo/W structure exhibits an increasing number of defects generated with increasing incident energy, while for the W/Mo structure this increase is much weaker. A probable explanation for these findings is the following one. In order to produce an extrinsic defect, for a given incident energy, an atom from the surface monolayer has to break the bonds between several bulk atoms and the bonds with its surface neighbors, a process considerably more expensive energetically compared with breaking the bonds between the surface atoms and creation of an intrinsic (surface in this case) defect. In the case when the E_c of the bulk atoms is larger, as compared to that of the monolayer atoms, the extrinsic defect formation energy is greater as compared to the opposite case. Thus, in our case study, when the monolayer consists of W atoms, the energy required to generate an extrinsic residual defect is considerably less than that required to produce the same damage when the monolayer consists of Mo atoms. However, as shown by the analysis of the EAC as a function of the atomic mass ratio, the incident energy plays its role in these processes, and so when the incident energy becomes sufficiently large, the metal with a higher EAC value will be the more likely candidate of generating extrinsic defects, in our case Mo. Our results suggest that this occurs somewhere between 150 and 200 eV for the Mo/W system. This is in agreement with experimental x-ray diffraction studies of the Mo/W system[15] showing that the W/Mo interface is broader by a factor of 2 than the Mo/W interface, for SL grown with Ar as the sputtering gas.

Based on our investigations of the sequence of atomic displacements generating different types of residual defects, as obtained from our simulations (Fig. 6), we propose the models[36] for point defect generation illustrated in Fig. 12. They are based on the following observations: (1) there is no evidence, in our simulations, of the incoming Ar atom penetrating any of the targeted structures deeper than between the monolayer and the first bulk layer at any value of the incident energy; (2) there is no Ar trapped in or on top of the structures; (3) both intrinsic and extrinsic defect generation are accompanied by Schottky-like and/or Frenkel-like pair formation; (4) there is no evidence in our simulations of interstitial extrinsic defect generation; i.e., no atom from the monolayer ends up as an interstitial in the bulk of the superlattice. Whole sequences of events occur only for high enough incident energies ($>$ 150 eV), when more defects are formed due to a single incoming atom. Figure 12(a) shows a process for impact point 1 where the atom hit by the Ar is pushed down into bulk layer two. The bulk accommodates this by moving the resulting interstitial along a close-packed direction, finally expelling an atom on the surface. In Fig. 12(b), an impact at point 3 results in a deep-lying interstitial in the same manner as shown in Fig. 3. The dynamics are the same in Fig. 12(c), but in this case the impact is at point 1 and results in an extrinsic substitutional defect as well. The process shown in Fig. 12(d) is typically occurring for impact points 2, 3, 4, and 5 at energies of at least 100 eV. Generally only parts of the sequences shown in Fig. 12 will be observed at lower energies, and a smaller number of defects will be generated.

IV. CONCLUSIONS

We report an investigation of the mechanisms responsible for residual point defect generation in Mo/W superlattices and the role played in these by the impact parameter, material combinations, and incident energy. In a growing superlattice, the situation where several monolayers of the same material have been grown can be regarded as a single metal case. For these cases, we find that the number of residual point defects created is well mapped by the values of the EAC. This means that the process of generating defects under these conditions is a mass-effect-dominated phenomenon. In contrast to this situation is the case when the growth of 1 ML, of the alternate, has been completed. Even though the value of the EAC of the whole structure is close to the EAC bulk value of the monolayer, the same pattern is not extended into the number of defects. This is especially true for the extrinsic defects, which are the types of defects mainly accountable for the intermixing of the interface. We find that at low enough energies, below 150 eV, for the Mo/W and W/Mo systems, the whole structure is influenced more by the bulk properties of the metal beneath the surface monolayer. By bulk properties we specifically refer to the characteristic defect formation energy of the metal, which is related to the cohesive energy.[37] At higher energies the mass effect will become predominant again and the whole structure will have defect formation properties similar to the monolayer.

ACKNOWLEDGMENTS

This work was financially supported by the Materials Research Consortium ''Thin Film Growth'' (financed by the Swedish Board for Technical Development, NUTEK, and the Swedish Natural Research Council, NFR) and the Swedish Research Council for Engineering Science (TFR), which is gratefully acknowledged. The authors would also like to express their gratitude to J. E. Sundgren, L. Hultman, J. Greene, I. Ivanov, and E. R. Svedberg for their support and many interesting and enlightening discussions.

[1] M. G. Karkut, D. Ariosa, J. M. Triscone, and Ø. Fischer, Phys. Rev. B **32**, 4800 (1985).
[2] M. G. Karkut, J. M. Triscone, D. Ariosa, and Ø. Fischer, Phys. Rev. B **34**, 4390 (1986).
[3] J. M. Triscone, D. Ariosa, M. G. Karkut, and Ø. Fischer, Phys. Rev. B **35**, 3238 (1987).
[4] D. Ariosa, Ø. Fischer, M. G. Karkut, and J. M. Triscone, Phys. Rev. B **37**, 2415 (1988).
[5] D. Ariosa, Ø. Fischer, M. G. Karkut, and J. M. Triscone, Phys. Rev. B **37**, 2421 (1988).
[6] M. R. Kahn, C. S. L. Chun, G. P. Felcher, M. Grimsditch, A. Kueny, C. M. Falco, and I. K. Schuller, Phys. Rev. B **27**, 7186 (1983).
[7] A. Hu, S. Zhang, X. Yuan, Q. Shen, Z. Lu, and D. Feng, Phys. Status Solidi A **107**, 153 (1988).
[8] J. L. Makous and C. M. Falco, Solid State Commun. **68**, 375 (1988).
[9] M. T. Pérez-Fríaz and J. L. Vicent, Phys. Rev. B **38**, 9503 (1988).
[10] J. M. Murduck, D. W. Capone, I. K. Schuller, S. Foner, and J. B. Ketterson, Appl. Phys. Lett. **52**, 504 (1988).
[11] G. Håkansson, J. Birch, L. Hultman, I. P. Ivanov, J.-E. Sundgren, and L. R. Wallenberg, J. Cryst. Growth **121**, 399 (1992).
[12] J. Birch, L. Hultman, J.-E Sundgren, and G. Radnoczi, Phys. Rev. B **53**, 8114 (1996).
[13] J.-E. Sundgren, L. Hultman, G. Håkanson, J. Birch, and I. Petrov, in *Materials Modification by Energetic Atoms and Ions*, edited by K. S. Grabowski *et al.*, MRS Symposia Proceedings No. 268 (Materials Research Society, Pittsburgh, 1992), pp. 71–82.
[14] E. B. Svedberg, Master thesis, Linköping University, Sweden, 1993.
[15] E. B. Svedberg, J. Birch, I. Ivanov, E. P. Münger, and J.-E. Sundgren (unpublished).
[16] M. Daw and M. I. Baskes, Phys. Rev. B **29**, 6443 (1984).
[17] E. Clementi, and C. Roetti, At. Data Nucl. Data Tables **14**, 177 (1974).
[18] R. A. Johnson and D. J. Oh, J. Mater. Res. **4**, 1195 (1989).
[19] R. A. Johnson, Phys. Rev. B **39**, 12 554 (1989).
[20] M. A. Tildesley and D. J. Tildesley, *Computer Simulation of Liquids* (Oxford University Press, Oxford, 1990).
[21] N. W. Ashcroft and N. D. Mermin, *Solid State Physics* (Saunders College, Philadelphia, 1988).
[22] E. P. Münger, Movie. The package allows the user to manipulate the graphic presentation of the crystal in real time. Options include but are not limited to rotations, scaling, color coding, and a two-dimensional cut of the three-dimensional simulation cell (unpublished).
[23] D. Hull and J. Bacon, *Introduction to Dislocations*, 3rd ed. (Pergamon, New York, 1984), Chap. 1.
[24] M. Knudsen, *The Kinetic Theory of Gases* (Methuen, London, 1934).
[25] F. O. Goodman and H. Y. Wachman, *Dynamics of Gas-Surface Scattering* (Academic, New York, 1976), Chap. 6.
[26] B. Baule, Ann. Phys. (Leipzig) **44**, 145 (1914).
[27] R. A. Oman, in *Rarified Gas Dynamics*, edited by C. L. Brundin (Academic, New York, 1967), p. 83.
[28] F. O. Goodman, *Rarified Gas Dynamics* (Ref. 27), p. 35.
[29] F. O. Goodman, Surf. Sci. **7**, 391 (1967).
[30] *American Institute of Physics Handbook* (McGraw-Hill, New York, 1957).
[31] C. Kittel, *Introduction to Solid State Physics*, 4th ed. (Wiley, New York, 1971), p. 96.
[32] G. Simmons and H. Wang, *Single Crystal Elastic Properties and Calculated Aggregate Properties: A Handbook*, 2nd ed. (MIT Press, Cambridge, MA, 1971).
[33] K. Maier, M. Peo, B. Saile, H. E. Schaefer, and A. Seeger, Philos. Mag. A **40**, 701 (1979).
[34] M. Tietze, S. Takaki, I. A. Schwirtlich, and H. Schultz, in *Point Defects and Defect Interaction in Metals*, edited by J.-I Takamura, M. Doyama, and M. Kiritani (North-Holland, Amsterdam, 1982), p. 266.
[35] R. Ziegler and H. E. Schaeefer, in *Vacancies and Interstitials in Metals and Alloys*, edited by C. Abromeit and H. Wollenberger (Trans Tech, Aedermannsdorf, Switzerland, 1987), p. 145.
[36] M. H. Carlberg, V. Chirita, and E. P. Münger, Nucl. Instrum. Methods **112**, 109 (1996).
[37] N. W. Ashcroft and N. D. Mermin, *Solid State Physics* (Ref. 21).